HHS Public Access

Author manuscript

Br J Pharmacol. Author manuscript; available in PMC 2023 October 01.

Published in final edited form as:

Br J Pharmacol. 2022 October ; 179(20): 4829–4843. doi:10.1111/bph.15915.

An *in silico-in vitro* pipeline for drug cardiotoxicity screening identifies ionic proarrhythmia mechanisms

Alexander P. Clark[1], **Siyu Wei**[2], **Darshan Kalola**[3], **Trine Krogh-Madsen**[4,5], **David J. Christini**[1,2]

[1]Department of Biomedical Engineering, Cornell University, Ithaca, NY 14853

[2]Department of Physiology and Pharmacology, SUNY Downstate Medical Center, Brooklyn, NY 11203

[3]Weill Cornell Medicine & Memorial Sloan Kettering Cancer Center Computational Biology Summer Program, New York, NY 10065

[4]Department of Physiology & Biophysics, Weill Cornell Medicine, New York, NY 10065

[5]Institute for Computational Biomedicine, Weill Cornell Medicine, New York, NY 10065

Abstract

Background and Purpose: Before advancing to clinical trials, new drugs are screened for their proarrhythmic potential using a method that is overly conservative and provides limited mechanistic insight. The shortcomings of this approach can lead to the misclassification of beneficial drugs as proarrhythmic.

Experimental Approach: An *in silico-in vitro* pipeline was developed to circumvent these shortcomings. A computational human induced pluripotent stem cell-derived cardiomyocyte (iPSC-CM) model was used as part of a genetic algorithm to design experiments, specifically

Corresponding Author: David Christini, SUNY Downstate Health Sciences University, 450 Clarkson Ave, Brooklyn, NY 11203, United States, 718-270-1681, David.Christini@downstate.edu.

Author contributions

A.C., T.K.M., and D.C. designed the study; A.C. and S.W. conducted experiments; A.C. and D.K. developed the optimization code; A.C. performed computational studies and statistical tests; A.C., S.W., T.K.M., and D.C. wrote the paper.

Conflict of interest statement

The authors declare no competing interest.

IKr: https://www.guidetopharmacology.org/GRAC/ObjectDisplayForward?objectId=572

IK1: https://www.guidetopharmacology.org/GRAC/ObjectDisplayForward?objectId=430&familyId=74&familyType=IC

Verapamil: https://www.guidetopharmacology.org/GRAC/LigandDisplayForward?ligandId=2406

Cisapride: https://www.guidetopharmacology.org/GRAC/LigandDisplayForward?ligandId=240

Quinidine: https://www.guidetopharmacology.org/GRAC/LigandDisplayForward?ligandId=2342

Quinine: https://www.guidetopharmacology.org/GRAC/ObjectDisplayForward?objectId=400

If: https://www.guidetopharmacology.org/GRAC/ObjectDisplayForward?objectId=400

IKs: https://www.guidetopharmacology.org/GRAC/ObjectDisplayForward?objectId=560

ICaL: https://www.guidetopharmacology.org/GRAC/ObjectDisplayForward?objectId=529

INa: https://www.guidetopharmacology.org/GRAC/ObjectDisplayForward?objectId=582

Ito: https://www.guidetopharmacology.org/GRAC/ObjectDisplayForward?objectId=554

HCN1: https://www.guidetopharmacology.org/GRAC/ObjectDisplayForward?objectId=400 (same as I_f)

electrophysiological voltage-clamp (VC) protocols, to identify which of several cardiac ion channels were blocked during *in vitro* drug studies. Such VC data, along with dynamically clamped action potentials (AP), were acquired from iPSC-CMs before and after treatment with a control solution or a low- (verapamil), intermediate- (cisapride or quinine), or high-risk (quinidine) drug.

Key Results: Significant AP prolongation (a proarrhythmia marker) was seen in response to quinidine and quinine. The VC protocol identified block of I_{Kr} (a source of arrhythmias) by all strong I_{Kr} blockers, including cisapride, quinidine, and quinine. The protocol also detected block of I_{CaL} by verapamil and I_{to} by quinidine. Further demonstrating the power of the approach, the VC data uncovered a previously unidentified I_f block by quinine, which was confirmed with experiments using a HEK-293 expression system and automated patch-clamp.

Conclusion and Implications: We developed an *in silico-in vitro* pipeline that simultaneously identifies proarrhythmia risk and mechanism of ion channel-blocking drugs. The approach offers a new tool for evaluating cardiotoxicity in the preclinical drug screening phase.

Graphical Abstract

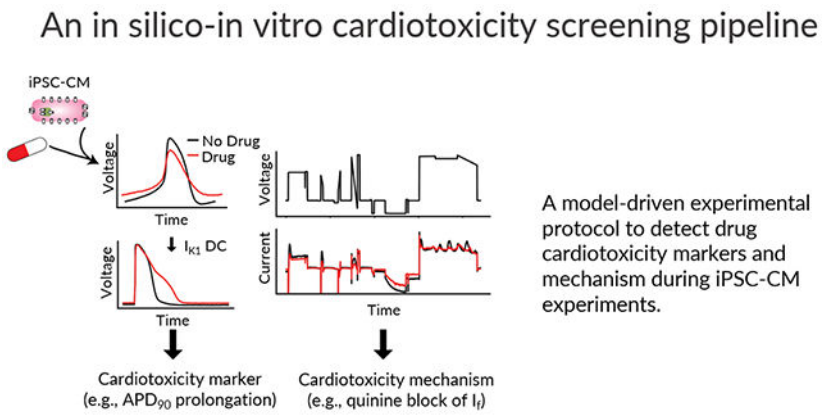

Keywords

Cardiotoxicity; Arrhythmias; Induced pluripotent stem cells; Preclinical drug evaluation; Computer simulation; Ion channels

Introduction

The use of *in vitro* IKr assays by regulatory agencies and pharmaceutical companies prevents the approval of lethal proarrhythmic drugs (Anonymous, 2005). However, the high sensitivity of such assays comes at the cost of low specificity (De Bruin et al., 2005; Hancox et al., 2008; Gintant, 2011), and have been shown to incorrectly label safe and effective therapies (e.g., verapamil and ranolazine) as proarrhythmic (Johannesen et al., 2014; Crumb et al., 2016).

To address these specificity shortcomings, the Comprehensive *in Vitro* Proarrhythmia Assay (CiPA) initiative was started in 2013 to guide the development of more accurate preclinical tests (Sager et al., 2014). The initiative recommended a three-step drug screening

approach that includes: 1) quantifying drug effects on the major cardiac ionic currents using expression system cells, 2) integrating these effects into *in silico* models and using simulations to evaluate a drug's proarrhythmic potential, and 3) validating simulations with human-derived induced pluripotent stem cell-derived cardiomyocytes (iPSC-CMs) and human ECG studies.

Over the last decade, drug effects on iPSC-CM action potential (AP) duration or field potential duration have become a common metric to evaluate drug risk (Navarrete et al., 2013; Blinova et al., 2018). iPSC-CMs however, are an imperfect model of adult physiology, with an immature phenotype, high degree of heterogeneity, and depolarized maximum diastolic potential (Goversen et al., 2018b). These features make it difficult to record consistent and reliable measures of proarrhythmia risk. Furthermore, the heterogeneity of these cells limits the ability to validate *in silico* simulations and can produce discrepancies between experimental and computational results (Paci et al., 2021a).

Dynamic clamp of a synthetic inward rectifier potassium current (IK1) into iPSC-CMs is a well-established method to improve the apparent electrophysiological maturity of cells for drug studies. The I_{K1} model current is calculated in real time and injected into iPSC-CMs to prevent spontaneous beating and establish a stable maximum diastolic potential below −65mV (Quach et al., 2018; Fabbri et al., 2019). When paced from this hyperpolarized resting membrane potential, cells have a more consistent, and adult-like AP phenotype, making drug-induced AP changes easier to interpret (Goversen et al., 2018a; Li et al., 2019).

In this study, we developed a pipeline that uses I_{K1} dynamic clamp and a novel voltage-clamp (VC) optimization approach to determine both the proarrhythmia risk and mechanism of a drug from iPSC-CM experiments. We start with *in vitro* iPSC-CM studies to determine drug block that we then confirm with expression system dose-response experiments. During the *in vitro* iPSC-CM studies conducted here, we acquired optimized VC data, along with I_{K1} dynamically clamped APs, before and after application of a CiPA-labeled low- (verapamil), intermediate- (cisapride), or high-risk (quinidine) drug or quinine, which is also known to be proarrhythmic (Woosley et al.; Colatsky et al., 2016). In addition to correctly identifying all three ion channels that were expected to be strongly blocked (>30%) by at least one of these drugs, the protocol also identified a previously unreported block of funny current (If) by quinine. This approach has potential as a new cardiotoxicity screening tool that can increase specificity, while also providing information about the underlying mechanism.

Methods

Pipeline design.

Figure 1 displays the steps of a cardiotoxicity screening pipeline that we developed and validated in this study. The first step in the pipeline is to use an *in silico* iPSC-CM model-guided genetic algorithm (GA) to design a VC protocol that isolates individual currents (Step 1). While the VC protocol could in principle be designed to isolate any of the ionic currents present in the *in silico* model, in this study we focused on seven currents that are most associated with AP morphology: I_{K1}, I_f, slow (IKs) and delayed (I_{Kr}) rectifier

potassium, L-type calcium (ICaL), sodium (INa), and transient outward (Ito). Optimized VC, as well as spontaneous and I_{K1} dynamic clamp and paced AP data, is acquired from a patient-derived iPSC-CM before and after drug application (Step 2). The I_{K1} dynamic clamp data is used to measure surrogate markers of cardiotoxicity (Step 3), while the optimized VC data is used to identify ion channel targets (Step 4). Dose-response data is then acquired for the identified targets using expression line cells (Step 5). For example, in this study we acquired the dose-response data for quinine block of HCN1, which further validated our findings on the unreported block of I_f by quinine.

Voltage clamp protocol optimization.

The baseline Kernik-Clancy iPSC-CM model was used in this study (Kernik et al., 2019). Experimental artifacts (e.g., seal leak, series resistance compensation, and voltage offset) were included in our model simulations following the simplified artifact model from Lei et al. (Lei et al., 2020). Taking experimental artifacts into account produce better fits of ion channel models to experimental data, while adjusting fewer parameters (Lei et al., 2020). The effects of these patch-clamp artifacts are particularly pronounced within the first few milliseconds after a voltage step (Figure S1). Prior to the VC protocol optimization, the model was run to steady state, and then simulated under voltage clamp at −80 mV for 20 s.

An optimized VC protocol was designed for each of seven currents (I_{Kr}, I_{CaL}, I_{Na}, I_{to}, I_{K1}, I_f, and I_{Ks}). Custom Python code that included the DEAP Python package was developed to implement the VC optimization GA (Fortin et al., 2012). The GA had 200 individual protocols per generation and 50 generations. Each protocol in the GA had a set of four voltage segments. Each segment could be either a step or ramp between 5 and 1000 ms long and was constrained to voltages between −120 and 60 mV.

To evaluate the fitness of a VC protocol, the Kernik-Clancy model with experimental artifacts was clamped, and the percent contribution (C(t)) of the target current was calculated at every timepoint.

$$C(t) = \frac{|I_x(t)|}{\sum_n |I_n(t)|}$$

In this equation, I_x is the target current. The denominator is the sum of the absolute values for all currents, including ionic currents and pipette leak (from the artifact equations). The best possible contribution score is equal to one and represents when the target current contributes all the current observed during a patch-clamp experiment. We calculated the average contribution, C(t), over a 10 ms window at each timepoint and used the highest contribution window value as the fitness score for the protocols.

Combining VC protocols.

The protocol with the highest current contribution for each of the seven ionic currents (Figures S2–S8) was combined into one large protocol. Before combining the protocols, they were systematically shortened using a two-step process. First, the portion of the protocol >50 ms after the maximum current contribution window, identified by the fitness

function, was removed. Then, 10 ms segments were incrementally removed from the beginning of the protocol, while ensuring the max current contribution did not decrease by more than 5%. The seven shortened protocols were connected by 500 ms holding steps at −80 mV. The 500 ms duration was chosen for two reasons: 1) it is long enough for many ion channel state variables to reach steady state and 2) the maximum contribution of each current did not decrease by more than 10% for any of the currents (Table SI).

To validate that the VC protocol isolates current during the same time windows in a cell with different conductance and kinetic parameters, the optimized VC protocol was applied to the Paci iPSC-CM model (Paci et al., 2018) with experimental artifacts. The VC protocol was also applied to the Kernik-Clancy model with extracellular Ca^{2+} concentration set to 1.2 mM, a value within the normal physiological range, but different from our extracellular patch-clamp solution. We found little difference in the amount of current isolation under these two conditions (Table SII).

iPSC-CM experiments.

Frozen vials of iPSC-CMs were thawed and cultured as a monolayer in one well of a 6-well plate precoated with 1% Matrigel and supplemented with RPMI media *(Fisher/Corning 10-040-CM*) containing 5% FBS (*Gibco 16000069*) and 2% B27 (*Gibco A1895601*). Cells were placed in an incubator at 37°C, 5% CO_2, and 85% humidity for 48 hours. When replating, cells were lifted with 1 mL Accutase (*Corning A6964*), and the enzymatic reaction was blocked with DMEM/F12 (*Gibco 10565-042*) plus 5% FBS (Burridge et al., 2014). Cells were diluted to 100,000 cells/mL and re-distributed to 124 sterile 8 mm coverslips precoated with 1% Matrigel. RPMI media was replaced every other day. Cells were patched from days 5 to 15 after thaw. Each cell in this study was acquired from a different coverslip that had been independently cultured for >4 days in a 24-well plate. Each cell was treated with drugs independently of all other cells in the study to produce independent experimental samples. Cells from five different vials were used in this study (see further details in the *Data analysis and statistics* section below).

Perforated patch-clamp experiments were conducted using borosilicate glass pipettes pulled to a resistance of 2-4 MΩ using a flaming/brown micropipette puller (Model P-1000; Sutter Instrument, Novato, CA). The pipettes were filled with intracellular solution containing 10 mM NaCl, 130 mM KCl, 1 mM $MgCl_2$, 10 mM $CaCl_2$, 5.5 mM dextrose, 10 mM HEPES. Amphotericin B was used as the perforating agent. Amphotericin B allows only monovalent ions to pass through the cell membrane, so a high intrapipette calcium concentration was used as a quality control step. In the case of an unintended rupture, calcium will diffuse into the cell and cause calcium-induced toxicity, which will terminate the experiment. The pipette tip was first dipped into intracellular solution with no amphotericin B for 2-5 s. Then, the pipette was backfilled with intracellular solution containing 0.44 mM amphotericin B. The coverslips containing iPSC-CMs were placed in the bath and constantly perfused with an extracellular solution at 35-37°C containing 137 mM NaCl, 5.4 mM KCl, 1 mM $MgSO_4$, 2 mM $CaCl_2$, 10 mM dextrose, 10 mM HEPES.

Patch-clamp measurements were made at 10kHz by a patch-clamp amplifier (Model 2400; A-M Systems, Sequim, WA) controlled by the Real Time eXperiment Interface (RTXI;

http://rtxi.org) to send commands to the amplifier via the data acquisition card (PCI-6025E; National Instruments, Austin, TX). After immersing the pipette into the extracellular solution, voltage was set to zero, and voltage offset in our recordings was assumed to be equal to the liquid junction potential of −2.8 mV. After contact with a cell was made and a seal of greater than 300 MΩ was established, we waited for the access resistance to decrease below 40 MΩ before starting experiments. A series resistance of 9-50 MΩ was obtained for all experiments, and series resistance compensation was set to 70%. The 70% compensation was chosen because larger values caused oscillations during the recordings.

Spontaneous, I_{K1} dynamic clamp, and VC data was acquired before and after drug application. Once access was gained, spontaneous behavior was acquired for >10 s. Dynamic clamp I_{K1} data was acquired using a custom RTXI module that implemented the Ishihara et al. model (Ishihara et al., 2009). A recent *in* silico study showed that the Ishihara model has properties that are optimal for use in I_{K1} dynamic clamp drug studies of iPSC-CMs (Fabbri et al., 2019). With this module, we injected 0.5x the baseline amount of Ishihara I_{K1}. If spontaneous behavior was not suppressed, and the resting membrane potential was above −65 mV, we incrementally increased the injected current by 0.25x or 0.5x of the baseline amount of Ishihara I_{K1} until these requirements were met. Resting at this hyperpolarized potential allows sodium channels to recover, resulting in APs with faster upstrokes and larger amplitudes, better resembling adult ventricular APs. The amount of I_{K1} dynamically clamped into a cell will influence its APD, which is why we chose to inject the minimum amount to suppress automaticity. The amount of I_{K1} dynamically clamped into each cell can be found in the data repository linked from the project GitHub page. The amount of I_{K1} injected into these cells (0.5-3x) is similar to modeled results with the Kernik-Clancy. After dynamic clamp data was acquired, the amplifier was switched to voltage clamp mode, and compensation of capacitance and access resistance was done. The cell was then clamped with the optimized VC protocol.

Following VC acquisition, the perfusion system was switched to an external solution containing either 0.1% of dimethyl sulfoxide (DMSO), or one of the following drugs: cisapride monohydrate at 250 nM, verapamil hydrochloride at 150 nM, quinidine at 2.7 μM, or quinine at 12 μM. Drug solutions were prepared daily, by dissolving in DMSO before dilution in external solution. The DMSO concentration was <0.1% for all drug solutions. The drug perfusion system was run for >5 minutes, while square pulses were applied to observe changes in the current response. Once the perfusion system had run for >5 minutes and changes in the current response had stabilized, spontaneous, I_{K1} dynamic clamp, and VC data was acquired.

HEK-HCN1 experiments.

Human embryonic kidney cells 293 with tetracycline-inducible expression of human hyperpolarization-gated cyclic nucleotide-sensitive cation channel 1 (HEK-HCN1) were cultured and maintained according to a protocol from Charles River. One frozen vial of cells was thawed in prewarm DMEM/F12 media plus 10% FBS and 100 units/ml Penicillin/Streptomycin *(Life Technologies 15140)* and placed in 37°C, 5% CO_2, and 85% humidity incubator overnight. The media was replaced with selection media containing 0.005 mg/mL

Blasticidin *(InvivoGen ant-bl-5b)* and 0.1 mg/mL Zeocin *(InvivoGen ant-zn-5b),* and the cells were sub-cultured if they were at ~ 75% confluency.

To induce expression of HCN1 channels, cells were cultured in DMEM/F12 media plus 1.5 μg/mL tetracycline *(Sigma-Aldrich T7660)* two days before the experiment. To prepare the cells for use in the Nanion Patchliner automated patch system, they were rinsed twice with 5 mL Hank's Balanced Salt solution *(Life Technologies 14175)* and lifted with 2 mL Accutase. The enzymatic reaction was blocked using DMEM/F12 media and the cell solution was centrifuged for 2 min. Supernatant was discarded and the cell pellet was mixed with FBS-free DMEM/F12 media plus 15 mM HEPES (pH 7.3) and extracellular solution. The cell mix solution was placed in a 4°C fridge for 10 min before use.

HEK-HCN1 current was recorded using an automated patch clamp system (Patchliner Quattro, Nanion Technologies GmbH), sampling at 25kHz. Whole cell patch clamp was performed at room temperature using standard medium resistance NPC-16 chips (1.8-3 MΩ) after getting a GΩ seal. Series resistance was compensated at 80% for VC recordings.

I_f current-voltage (I-V) traces were recorded starting from a holding potential of −20mV. Cells were stepped to a potential between −20 mV and −120 mV for 3500 ms, decreasing by 10 mV steps, and then stepped to −50 mV for 500 ms to acquire the tail current. Maximum currents were calculated as the average current over the last 800 ms of the hyperpolarizing step. Maximum tail currents were calculated as the average between 8 and 16 ms after the step to −50 mV.

To measure the dose-response of HCN1 current treated with quinine, peak currents were measured by stepping from a holding potential of −20 mV to −110 mV for 3500 ms. This data was acquired under each of the following conditions, in this order: no drug, 0.5% DMSO in external (the maximum DMSO concentration), and then 1 μM, 4 μM, 12 μM, 40 μM, 200 μM, 400 μM, and 800 μM quinine in external. Maximum currents were calculated as the average current over the last 800 ms of the hyperpolarizing step. These traces were acquired three or four times at each dose. The last two traces at each dose, which were acquired >40 s after drug application, were used for analysis. Each data point plotted in Figure 7C is an average of the currents from these two traces.

In all experiment, cells were measured using extracellular solution with the following concentrations (in mM): 140 NaCl, 4 KCl, 2 CaCl2, 1 MgCl2, 5 D-Glucose monohydrate, 10 HEPES, pH adjusted to 7.4 with NaOH, and 298 mOsm. The intracellular solution had the following concentrations (in mM): 10 EGTA, 10 HEPES, 10 KCl, 10 NaCl, 110 KF, pH 7.2 with KOH, 280 mOsm.

Data analysis and statistics.

All results are presented as mean ± standard error of the mean. All cells that lasted until the end of an experiment and had a seal greater than 300 MΩ before perforation and access below 50 MΩ were included in this study. In total, 40 iPSC-CMs were analyzed in this study. We compared changes in AP features and VC current traces from iPSC-CM data

acquired before and after application of cisapride (n=6), verapamil (n=9), quinidine (n=6), quinine (n=9), or a DMSO control solution (n=10).

For each drug, a single iPSC-CM vial was thawed and experiments were conducted with either the drug of interest or a DMSO control solution between 5 and 15 days after the thaw. On a given day, all trials were conducted with either the DMSO control or drug solution. Information about patched cells was not used to select the perfusion solution (e.g., randomization). Data was analyzed after day 15, and cells that did not meet our quality control thresholds for seal and access resistance were removed. An additional vial was thawed if n<6. A single thaw was enough to meet these standards for verapamil, quinidine, and quinine. Two vials were required for cisapride. The DMSO control group includes cells from all the thawed vials. The experimentalist was not blinded to the drugs used. This was not required, as the analysis and quality control thresholds were established *a priori*, with one exception (see discussion of I_{Kr} segment). Statistical tests were conducted after all data was collected.

Significant differences between the DMSO and each drug group were calculated using the SciPy unpaired t-test function in Python, with significance indicating $p<0.05$. Significance was calculated to compare I_{K1} dynamic clamp AP prolongation. For the VC data, significance was calculated over the seven regions that the Kernik-Clancy model identified as maximizing the isolation I_{Kr}, I_{Na}, I_{CaL}, I_{to}, I_{K1}, I_f, and I_{Ks}. The goal was to identify time windows over which ionic currents were isolated and use the occurrence of current reduction in individual cells within those windows to identify drug block. The precise p value for each statistical test is presented in its corresponding figure. Confidence intervals are set to 95% for each point plot. All statistical analyses were performed using the raw experimental data. For presentation in figures, data were smoothed with a 0.4 ms moving average.

A functional t-test (Keser, 2014) was used to determine the time windows when current response changes to drug treatment differed from responses to DMSO treatment. We used the following steps to develop a null distribution, conduct a t-test at every timepoint, and determine windows of significant difference between DMSO control and drug groups:

1. For both the control and drug groups, we calculated the change in current at every timepoint from pre- to post-treatment.
2. We developed a null distribution by completing the following step 200 times: we combined and randomly shuffled individuals from the drug and control groups, and then redistributed them into two distinct groups. We calculated a T-statistic (T(t)) at every timepoint.
3. We found the t-value at the 95^{th} quantile of the null distribution and used it as the threshold for determining significant differences between our control and drug groups. In other words, the control and drug groups were labeled significantly different at a time when the T-value comparing these two groups was greater than the T-value at the 95^{th} percentile of the null distribution.

The windows plotted in Figures 5, 6, and S10–S13 show where there is a significant difference between the drug and DMSO groups that lasts for more than 1 ms. The functional

t-test calculations were completed with custom Python code using the SciPy unpaired t-test function.

The data and statistical analyses in this paper comply with the recommendations of the *British Journal of Pharmacology* on experimental design and analysis in pharmacology (Curtis et al., 2018).

Materials.

Cisapride monohydrate and quinine were obtained from Sigma Aldrich (Saint Louis, MO). Verapamil hydrochloride was obtained from MP Biomedicals (Solon, OH). Quinidine was obtained from Tocris (Bristol, UK). Frozen stocks of human iPSC-CMs from a healthy individual (SCVI-480CM) were obtained from Joseph C. Wu, MD, PhD at the Stanford Cardiovascular Institute Biobank. The iPSC-CM line was derived from an African American female donor, and was approved by Stanford University Human Subjects Research Institutional Review Board. The cells were differentiated to cardiomyocytes as described previously (Churko et al., 2013; Burridge et al., 2014). HEK-HCN1 (CT6114) cells were obtained from Charles River (Wilmington, MA).

Code and data availability.

All code has been made publicly available on GitHub at: https://github.com/Christini-Lab/vc-optimization-cardiotoxicity. All the data presented in this manuscript has been made publicly available through Cornell eCommons.

Nomenclature of Targets and Ligands.

Key protein targets and ligands in this article are hyperlinked to corresponding entries in

http://www.guidetopharmacology.org, and are permanently archived in the Concise Guide to PHARMACOLOGY 2021/22 (Alexander et al., 2021).

Results

Optimizing a VC protocol to isolate individual currents for drug cardiotoxicity screening.

We used a GA to optimize VC protocols that maximize the current contribution for each of seven ionic currents: I_{Kr}, I_{CaL}, I_{Na}, I_{to}, I_{K1}, I_{Ks}, and I_f (Figure 2A, S2–S8). The VC protocols were systematically shortened and then combined into a single protocol that contained the segments that maximized the isolation of each ionic current (Figure 2B). The resulting protocol (~9 seconds) is short enough to be run multiple times in each cell under control conditions and after drug application.

We validated the VC protocol by applying it to a different iPSC-CM model (Paci et al., 2018) and comparing the windows of maximum current (Figure S9). This validation step provided us with confidence that the VC protocol could isolate currents during the same time windows from cells with different conductances and kinetics.

Synthetic maturation of iPSC-CMs by I_{K1} dynamic clamp improves interpretability of iPSC-CM AP data.

The iPSC-CMs displayed a heterogeneous spontaneous phenotype (Figure 3A), which is consistent with previous work on single-cell iPSC-CMs (Garg et al., 2019). To recover consistent AP data from all cells, we injected a synthetic I_{K1} model current (Ishihara et al., 2009) and paced the cells at 1Hz (Figure 3B). This data is consistent with previous work showing that I_{K1} dynamic clamp can reduce (although not eliminate) cell-to-cell heterogeneity while eliciting more adult-like AP behavior from iPSC-CMs (Li et al., 2019). The I_{K1} dynamic clamp and paced APs (n=40) had an average resting membrane potential of −74.2 ± 2.8 mV (Figure 3C) and action potential duration at 90% repolarization of 142.0 ± 48.3 ms (Figure 3D).

I_{K1} dynamic clamp AP data identifies surrogate markers of cardiotoxicity.

We compared changes in AP features for iPSC-CM data acquired before and after application of cisapride (n=6), verapamil (n=9), quinidine (n=6), quinine (n=9), or a DMSO control solution (n=10). Table 1 shows the percent block of each cardiac ion channel by these drugs based on previously published results (Crumb et al., 2016). Cisapride is a CiPA-labeled intermediate-risk drug and blocks I_{Kr} specifically at the concentration used in this study (50x the effective free plasma concentration, EFPC). The cell in Figure 4A did not show AP prolongation after cisapride treatment, which was the case for four of six cells. Verapamil is a low-risk drug that moderately blocks I_{CaL} and lightly blocks I_{Kr} at the concentrations used in this study (3xEFPC). Figure 4B shows a verapamil-treated cell that displays slight shortening during the plateau phase, which is characteristic of I_{CaL} block. Quinidine and quinine are both proarrhythmic and block multiple ion channels with a strong affinity for I_{Kr} at concentrations used in this study (3xEFPC). Both example quinidine- (Figure 4C) and quinine-treated (Figure 4D) cells show AP prolongation characteristic of such I_{Kr} block.

When compared to control, verapamil-treated cells showed shortening in the action potential duration at 20% of repolarization (APD_{20}), but the difference was not statistically significant (p=.056, Figure 4E). Cells that were treated with quinidine (p=.034) and quinine (p=.0003) showed a significant prolongation in the action potential duration at 90% of repolarization (APD_{90}) when compared to control cells (Figure 4F). Because APD_{90} prolongation is an established proarrhythmia risk indicator, these findings agree with the CiPA classification or known proarrhythmia risk for verapamil (low risk), quinidine (high risk), and quinine (conditional risk) at 3x their EFPC. Cisapride-treated cells did not show a significant change in APD_{90}, despite it being a stronger I_{Kr} blocker than quinidine and quinine at the concentrations used in this study. This may be because quinidine and quinine block other outward potassium currents, including I_{Ks}, at the concentrations used in this study. Such block of both dominant repolarizing potassium currents (I_{Kr} and I_{Ks}) may cause greater and more consistent AP prolongation in such a heterogeneous iPSC-CM population.

The optimized VC protocol qualitatively identifies drugs that block greater than 30% of an ionic current.

To identify the ion channel targets of each drug (i.e., mechanism), we compared the average change in VC responses from each drug treatment group to the DMSO control group. Because the protocol was designed to isolate specific ionic currents during brief windows of the protocol, changes in each of these seven segments could reveal ionic mechanism.

Figure 5A shows a representative example of a cell that was treated with quinine. The zoomed-in panel in Figure 5B shows the portion of the VC protocol that maximized the current contribution of I_{Kr} relative to the total current. This inset shows a decrease in the total current present after treatment with. The difference is particularly pronounced from 1260 ms to 1270 ms, the segment where I_{Kr} is predicted by the model to have a large relative contribution compared to the other ionic currents present. According to our modeling work, 1265-1270 ms is predicted to have the largest amount of I_{Kr}, however, the experimental data from this region was highly variable due to variations in access resistance among cells. We chose, instead, to focus on the 1260-1265 ms window, because it has the second largest I_{Kr} current isolation and is a few milliseconds after a voltage step, so access resistance has less of an effect on this region. Figure 5C shows the change in current during the window from 1260 ms to 1265 ms for all cells in this study.

Cells treated with cisapride, quinidine, and quinine all showed significant reductions in current during this segment compared to control cells. Cells treated with verapamil, a weaker I_{Kr} blocker at the concentration used here (21%), did not show a significant difference in current during this segment. These data suggest that the VC protocol can detect strong I_{Kr} block during the model-designed I_{Kr} isolation segment but fails to detect weak block of I_{Kr} current.

In addition to focusing on the model-identified segments of the protocol, we also performed a functional t-test to compare the average change in total current between control and drug-treated cells at every timepoint during the VC protocol.

Figure 5D through 5F shows the segment of the VC protocol where I_{Kr} should be isolated. The bottom panel shows the average change in membrane current ($\mu\Delta I_m$) at each timepoint for cells treated with cisapride (Figure 5D, cyan), quinidine (Figure 5E, green), or quinine (Figure 5F, blue). The black line in each of these panels shows the average change in cells treated with a DMSO control solution. The shaded window on the top of each panel shows the timepoints where there is a significant difference ($p<.05$) between control and treatment groups. The functional t-test identifies a significant difference in the currents between 1260 ms and 1265 ms for all three of these I_{Kr} blockers. There was no significant difference between DMSO and verapamil during this period. We plotted these significance windows over the entire VC protocol and compared them to individual currents from the Kernik-Clancy model (Figures S10–S13). Figures S10, S12, and S13 show significant differences throughout the regions where the Kernik-Clancy I_{Kr} current is present.

We conducted the same statistical analysis as shown in Figure 5C to determine changes during the isolating segments for each of the other currents. These isolating segments

correspond to the time windows of the VC protocol that maximized the isolation of each current in the Kernik-Clancy model (Figure S9). The boxes marked with (*) in Table 1 indicate currents that were identified as blocked based on significant changes in current during the corresponding model-identified segment. In addition to the I_{Kr} blocks noted above, the VC protocol correctly identified verapamil block of I_{CaL} and quinidine block of I_{to}. The VC protocol did not identify any reductions in I_{Na}, I_{K1}, or I_{Ks}, which were all weakly blocked by at least one of these drugs. Importantly, all blocks of more than 30% were correctly identified, and there were no currents that were incorrectly identified as being blocked. Taken with dynamic clamp AP data, these results indicate that the optimized VC protocol can be used to identify underlying currents responsible for changes in AP morphology.

The optimized VC protocol identifies a previously unreported quinine block of I_f.

As Table 1 indicates, quinine-treated iPSC-CMs revealed a previously unreported block of I_f. A representative cell trace shows, after quinine treatment, a net positive shift in membrane current throughout the region where the Kernik-Clancy model predicts I_f is present (Figure 6A, B). This positive shift in membrane current is consistent with I_f block. The areas of significant difference in this part of the protocol closely align with the Kernik-Clancy simulated I_f current (Figure 6C). This holds largely true both for when I_f is predicted to conduct an inward current (between 4400 ms and 6400 ms) and an outward current (between 6400 ms and 6600 ms). When we consider only the segment of the protocol where I_f current isolation is maximized, we find a significant increase in total current due to reduction of negative I_f, when compared to control cells (Figure 6D).

To verify the finding that quinine blocks I_f, we used a HEK-293 cell line with tetracycline-inducible expression of HCN1, the ionic channel that conducts I_f. We chose the HCN1 isoform because it was recently shown to be present at high densities in iPSC-CMs (Giannetti et al., 2021). Figure 7A, B show that these HCN1 cells have typical current-voltage I_f behavior. We acquired dose-response data under baseline external conditions, after treatment with a DMSO control solution, and at seven concentrations of quinine (Figure 7C, D). There was no significant difference between the traces acquired before and after the addition of a 0.5% DMSO control solution ($p>0.05$). The best fit Hill equation curve has an IC50 of 34.2 μM and Hill coefficient of 0.72. At 12 μM, which was the concentration used in the iPSC-CM study, the estimated block is 32.0%. Overall, this dose-response data confirms the findings from our iPSC-CM study, that quinine blocks I_f at 3x the EFPC.

Discussion

In this study, we demonstrated the potential of a drug screening pipeline that uses iPSC-CMs to simultaneously identify drug cardiotoxicity markers and mechanism. The pipeline relies on a novel optimization algorithm to produce VC protocols that we can use to identify multi-channel drug block that provide a mechanistic insight into AP morphology changes. We found that quinidine and quinine, both proarrhythmic drugs, caused AP prolongation. From the VC data, we correctly identified the four ion channels that were blocked by more than 30%. The VC protocol also uncovered a previously unreported block of I_f by quinine

in iPSC-CMs. A similar block was recently demonstrated in iPSC-derived neurons (Zou et al., 2018). We confirmed these findings with a dose-response study on an HCN1 expression system and found that quinine blocked the pore domain of I_f by 32% at the concentration used in this experiment.

Optimizing VC protocols for iPSC-CM drug experiments.

Traditional VC protocols are developed manually and typically designed to fit and/or measure specific model parameters (Hobbs and Hooper, 2008; Groenendaal et al., 2015; Beattie et al., 2018). The current study is a departure from this approach in two ways: 1) the protocols were designed automatically using a model-guided optimization, and 2) the resulting protocols were specifically designed to identify drug targets, not to improve fits. Due to the conserved nature of ion channels across various tissues, this new approach to protocol design is extensible to toxicity applications of other electrically excitable cells (e.g., neurons).

The success of such a VC protocol optimization requires reasonable agreement between the computational model (e.g., Kernik-Clancy) and *in vitro* cells (e.g., iPSC-CMs from Stanford Biobank). While the model in this study was able to create VC protocols that could detect strong ionic current blocks, the heterogeneity within the iPSC-CM population (Figure 3) indicates that the model does not fully capture the dynamics of the cells used here. Despite this discrepancy, the success of our *in vitro* experiments validates that the Kernik-Clancy model kinetics are descriptive enough of the iPSC-CMs we used to identify when currents are isolated during voltage clamp. This novel application of the model to optimize experiments differs from previous uses of iPSC-CM models, which have largely focused on predicting drug cardiotoxicity (Gong and Sobie, 2018; Tveito et al., 2018; Jæger et al., 2021) and screening channel mutations (Kernik et al., 2020) through *in silico* simulations. To the best of our knowledge, this is the first work that shows how *in silico* models can be used to improve the design, and therefore impact, of cardiotoxicity drug studies. Additionally, we believe the accuracy of the VC protocol optimization approach will improve with models developed to closely reflect the dynamics of the cell lines used in the cardiotoxicity studies.

Generating VC protocols that take advantage of the unique gating kinetics for each channel.

The GA was designed to isolate individual currents, thereby producing protocols (Figure 2A) that exploit the unique gating kinetics for each ion channel. For example, the I_{Kr} protocol (Figure S5) takes advantage of the fast-inactivation, slow-activation gating that is characteristic of this channel. The initial step to just above 0 mV inactivates the channel while the activation gate opens. The step to −40 mV opens the inactivation gate, allowing current to flow through the channel before the slower activation gate closes. The final step, back to more depolarized than 0 mV, increases the driving force, which provides a brief window (about 5 ms) where the activation gate is open, the inactivation gate is open, and there is a large driving force pushing potassium out of the cell.

The other protocols also identified dynamic ranges that highlight each channel's unique kinetics. The I_{Ks} (Figure S7) and I_f (Figure S8) protocols settle into positive (>50 mV) and negative (<−110 mV) extremes where most other channels are closed, but these channels are open and remain open. The I_{K1} protocol (Figure S6) isolates its current at the same potential as I_f, but is maximized before I_f has a chance to open. The I_{Na} protocol (Figure S2) steps to a hyperpolarized potential (−87 mV) to fully open the inactivation gate and then jumps to a ramp that is depolarized enough to activate the channel (−50 mV), while minimizing the activation of other ion channels (e.g., I_{CaL}). The I_{CaL} and I_{to} channels have fast activation and slow inactivation kinetics – these protocols take advantage of this by stepping to potentials that will open their channels but minimize the contribution from the other currents.

Screening for drug cardiotoxicity using the novel VC protocol and iPSC-CMs.

The existence of overly conservative cardiotoxicity screening guidelines points to the need to develop new methods that improve specificity and provide insight into the mechanism of drug block. In recent years, high throughput iPSC-CM screening approaches that rely on surrogate markers of cardiotoxicity risk have improved prediction accuracy and the ability to evaluate drugs at scale (Bedut et al., 2016; Lu et al., 2019; Pioner et al., 2019). Expression system cell lines and molecular-dynamic simulations have supplemented these findings by providing detailed single-channel mechanisms of drug action (Demarco et al., 2020; Yang et al., 2020). However, there have been few methods that provide both measures of cardiotoxicity and mechanism from the same iPSC-CM cells.

One recent approach fit an iPSC-CM model to voltage and fluorescent calcium AP data acquired before and after drug application (Tveito et al., 2018; Jæger et al., 2021). Because this approach only considers spontaneous AP and conduction velocity data, successful estimates of current block is limited to the currents that are sensitive to changes in these data (e.g., I_{Kr}, I_{CaL}, and I_{Na}).

Here, we built upon this work by developing an approach that provides both surrogate measures of drug cardiotoxicity and identification of drug block for seven cardiac ion channels. Our *in vitro* AP results showed significant prolongation of quinidine- and quinine-treated cells, which indicates their proarrhythmic potential at 3xEFPC. The VC protocol identified strong block of outward potassium currents by both quinidine (I_{Kr} and I_{to}) and quinine (I_{Kr} and I_f) which may explain such AP prolongation. Cisapride did not cause significant prolongation, however, the VC protocol correctly identified its block of I_{Kr}. This result indicates the value that the VC protocol has in detecting proarrhythmic mechanisms in the absence of cardiotoxic markers. If such a discrepant finding were identified from this pipeline, we would still label the drug as likely proarrhythmic based on block of I_{Kr}.

I_f is not often linked to repolarization in iPSC-CMs, however, we think it is likely playing a role in the cells from this study. I_f appears to be a relatively large current in these cells (Figure 6). Therefore, even if a small fraction of the channels are turned on during AP repolarization, as was recently shown in mouse sinoatrial node myocytes (Peters et al., 2021), I_f block could lead to AP prolongation. Additionally, the cells in this study had

relatively short APs (Figure 3D), so repolarizing I_f would be active for a greater proportion of the AP duration, before it turns off. However, this finding needs to be further validated.

Limitations and future directions.

This study has several limitations that will need to be addressed before this pipeline can be broadly implemented. First, before this approach can be used at scale, it should be validated with a high-throughput automated patch-clamp system. With this type of system, data could be acquired 10-100x faster at multiple drug concentrations and by operators who do not need the specialized patch-clamp skill. Such studies would produce a greater quantity of data with consistent experimental artifact parameters (Goversen et al., 2018a), resulting in less variability and greater power for statistical analyses.

Second, the VC protocol does not provide information about drug effects on channel kinetics and is designed to identify pore block of channels in a limited dynamic range. Designing an algorithm to tease apart such effects is a nontrivial extension of this project, and would need a target objective that is, likely, very different from the one used in this study.

Third, the cisapride-treated iPSC-CMs did not show significant prolongation, despite the VC protocol correctly identifying a strong block of I_{Kr}. Unlike cisapride, the quinidine- and quinine-treated cells showed significant AP prolongation. This discrepancy would occur if I_{Kr} were not the dominant repolarizing ionic current in the cells used in this study, as quinidine and quinine block other potassium currents in addition to I_{Kr}. Simultaneous block of these currents would deplete the repolarization reserve and cause more consistent AP prolongation from such a heterogeneous population.

Fourth, the iPSC-CMs often produced an oscillatory current trace when held at large positive voltages, which is likely caused by calcium overload that can occur at high potentials. This oscillatory pattern could decrease the sensitivity of the protocol to determine strong I_{Ks}-blockers, which we plan to test in the future.

Fifth, while we have shown that the protocol can identify strong block of four ion channels (I_{Kr}, I_{CaL}, I_f, and I_{to}) with no false positives, further validation of the approach is needed using drugs that block the remaining ion channels known to exist in iPSC-CMs (I_{Na}, I_{K1}, and I_{Ks}). Because the VC protocol was designed using the same model and GA, we are hopeful that it will work with these ion channels as well.

Sixth, we did not account for the effect that cell-to-cell variation and changes in series resistance have on the interpretation of current responses. Such variations can make it difficult to interpret current traces within 1 ms after a voltage step. For example, we measured changes from the second most-isolated I_{Kr} segment, because the peak occurred just after stepping to a new voltage. In the future, this issue may be avoided by adjusting the GA fitness function to exclude contribution calculations just after voltage steps. Such an approach could be validated with a set of iPSC-CM models that approximate the heterogeneity seen in experiments. One could simulate this heterogeneity by adjusting conductances and developing hybrid populations with currents from both the Paci and Kernik-Clancy models, as suggested in Paci et al. (2021b).

Finally, we would reproduce this study with cells from multiple donors. We do not expect donor demographics to have a meaningful effect on the success of this approach, as iPSC-CMs currently do not represent physiological differences between female vs. male adult cardiomyocytes well (Huo et al., 2019). However, patient-to-patient variations in ion channel expression levels could impact the extent of pre- to post-drug electrophysiological changes.

Conclusion.

In this study, we outline a new pipeline for determining drug cardiotoxicity and underlying mechanism by applying a novel VC protocol and I_{K1} dynamic clamp to iPSC-CMs. This pipeline correctly identified the ion channels that were strongly blocked by each drug, and identified proarrhythmic markers (e.g., AP prolongation) or mechanism (e.g., I_{Kr} block) for the intermediate- and high-risk drugs tested in this study. We think that this cardiotoxicity pipeline could have far-reaching effects on how drugs are screened and could ultimately increase the number of safe and effective drugs available to patients.

Supplementary Material

Refer to Web version on PubMed Central for supplementary material.

Acknowledgments

We thank Dr. Drew Tilley for his experimental insights and expertise. We thank Dr. Sumanta Basu for consulting on the functional t-test and Dr. Henry Sutanto for feedback on the manuscript. Please note that this manuscript has also been posted as a preprint on bioRxiv: https://www.biorxiv.org/content/10.1101/2021.09.10.459625. Research reported in this publication was supported by the National Heart, Lung, And Blood Institute of the National Institutes of Health under Award Number F31HL154655 (to A.C.) and U01HL136297 (to D.J.C.).

Declaration of transparency and scientific rigour

This Declaration acknowledges that this paper adheres to the principles for transparent reporting and scientific rigour of preclinical research as stated in the BJP guidelines for Design and Analysis, and as recommended by funding agencies, publishers and other organiations engaged with supporting research.

Data availability

Data that support the findings of this study are available through eCommons at https://doi.org/10.7298/c883-s773.

Abbreviations

iPSC-CM	Induced pluripotent stem cell-derived cardiomyocytes
AP	Action potential
APD_{20}	Action potential duration at 20% of repolarization
APD_{90}	Action potential duration at 90% of repolarization
CiPA	Comprehensive *in Vitro* Proarrhythmia Assay
VC	Voltage clamp

EFPC	Effective free plasma concentration
I_{Kr}	Rapid delayed rectifier K^+ current
I_{Ks}	Slow delayed rectifier K^+ current
I_{to}	Transient outward K^+ current
I_{K1}	Inward rectifier K^+ current
I_f	Funny current
I_{CaL}	L-type Ca^{2+} current
I_{Na}	Na^+ current

References

Alexander SP, Mathie A, Peters JA, Veale EL, Striessnig J, Kelly E, et al. (2021). The Concise Guide to PHARMACOLOGY 2021/22: Ion channels. Br. J. Pharmacol 178 Suppl: S157–S245. [PubMed: 34529831]

Anonymous (2005). ICH S7B Note for Guidance on the Nonclinical Evaluation of the Potential for Delayed Ventricular Repolarization (QT Interval Prolongation) by Human Pharmaceuticals. Int. Conf. Harmon. Tech. Requir. Regist. Pharm. Hum. Use.

Beattie KA, Hill AP, Bardenet R, Cui Y, Vandenberg JI, Gavaghan DJ, et al. (2018). Sinusoidal voltage protocols for rapid characterisation of ion channel kinetics. J. Physiol 596: 1813–1828. [PubMed: 29573276]

Bedut S, Seminatore-Nole C, Lamamy V, Caignard S, Boutin JA, Nosjean O, et al. (2016). High-throughput drug profiling with voltage-and calcium-sensitive fluorescent probes in human iPSC-derived cardiomyocytes. Am. J. Physiol. - Hear. Circ. Physiol 311: H44–H53.

Blinova K, Dang Q, Millard D, Smith G, Pierson J, Guo L, et al. (2018). International Multisite Study of Human-Induced Pluripotent Stem Cell-Derived Cardiomyocytes for Drug Proarrhythmic Potential Assessment. Cell Rep. 24: 3582–3592. [PubMed: 30257217]

Bruin M.L. De, Pettersson M, Meyboom RHB, Hoes AW, and Leufkens HGM. (2005). Anti-HERG activity and the risk of drug-induced arrhythmias and sudden death. Eur. Heart J 26: 590–597. [PubMed: 15637086]

Burridge PW, Matsa E, Shukla P, Lin ZC, Churko JM, Ebert AD, et al. (2014). Chemically Defined and Small Molecule-Based Generation of Human Cardiomyocytes. Nat Methods 11: 855–860. [PubMed: 24930130]

Churko JM, Burridge PW, and Wu JC (2013). Cellular Cardiomyoplasty: Methods and Protocols, Methods in Molecular Biology. 1036: 81–88. [PubMed: 23807788]

Colatsky T, Fermini B, Gintant G, Pierson JB, Sager P, Sekino Y, et al. (2016). The Comprehensive in Vitro Proarrhythmia Assay (CiPA) initiative — Update on progress. J. Pharmacol. Toxicol. Methods 81: 15–20. [PubMed: 27282641]

Crumb WJ, Vicente J, Johannesen L, and Strauss DG (2016). An evaluation of 30 clinical drugs against the comprehensive in vitro proarrhythmia assay (CiPA) proposed ion channel panel. J. Pharmacol. Toxicol. Methods 81: 251–262. [PubMed: 27060526]

Curtis MJ, Alexander S, Cirino G, Docherty JR, George CH, Giembycz MA, et al. (2018). Experimental design and analysis and their reporting II: updated and simplified guidance for authors and peer reviewers. Br. J. Pharmacol 175: 987–993. [PubMed: 29520785]

Demarco KR, Yang P-C, Singh V, Furutani K, Dawson J, Jeng M-T, et al. (2020). Molecular determinants of pro-arrhythmia proclivity of d- and l- sotalol via a multi-scale modeling pipeline. J. Mol. Cell. Cardiol 115800.

Fabbri A, Goversen B, Vos MA, Veen T.A.B. van, and Boer T.P. de (2019). Required GK1 to Suppress Automaticity of iPSC-CMs Depends Strongly on IK1 Model Structure. Biophys. J 117: 2303–2315. [PubMed: 31623886]

Fortin FA, Rainville F.M. De, Gardner MA, Parizeau M, and Gagńe C. (2012). DEAP: Evolutionary algorithms made easy. J. Mach. Learn. Res 13: 2171–2175.

Garg P, Oikonomopoulos A, Chen H, Li Y, Lam CK, Sallam K, et al. (2019). Genome Editing and Induced Pluripotent Stem Cells in Cardiac Channelopathy. J. Am. Coll. Cardiol 72: 62–75.

Giannetti F, Benzoni P, Campostrini G, Milanesi R, Bucchi A, Baruscotti M, et al. (2021). A detailed characterization of the hyperpolarization-activated 'funny' current (If) in human-induced pluripotent stem cell (iPSC)-derived cardiomyocytes with pacemaker activity. Pflugers Arch. 473: 1009–1021. [PubMed: 33934225]

Gintant G (2011). An evaluation of hERG current assay performance: Translating preclinical safety studies to clinical QT prolongation. Pharmacol. Ther 129: 109–119. [PubMed: 20807552]

Gong JQX, and Sobie EA (2018). Population-based mechanistic modeling allows for quantitative predictions of drug responses across cell types. Npj Syst. Biol. Appl 4:.

Goversen B, Becker N, Stoelzle-Feix S, Obergrussberger A, Vos MA, Veen T.A.B. van, et al. (2018a). A hybrid model for safety pharmacology on an automated patch clamp platform: Using dynamic clamp to join iPSC-derived cardiomyocytes and simulations of Ik1 ion channels in real-time. Front. Physiol 8: 1–10.

Goversen B, Heyden M.A.G. van der, Veen T.A.B. van, and Boer T.P. de (2018b). The immature electrophysiological phenotype of iPSC-CMs still hampers in vitro drug screening: Special focus on IK1. Pharmacol. Ther 183: 127–136. [PubMed: 28986101]

Groenendaal W, Ortega FA, Kherlopian AR, Zygmunt AC, Krogh-Madsen T, and Christini DJ (2015). Cell-Specific Cardiac Electrophysiology Models. PLoS Comput. Biol 11: 1–22.

Hancox JC, McPate MJ, Harchi A. El, and Zhang Y. hong (2008). The hERG potassium channel and hERG screening for drug-induced torsades de pointes. Pharmacol. Ther 119: 118–132. [PubMed: 18616963]

Hobbs KH, and Hooper SL (2008). Using complicated, wide dynamic range driving to develop models of single neurons in single recording sessions. J. Neurophysiol 99: 1871–1883. [PubMed: 18256169]

Huo J, Wei F, Cai C, Lyn-Cook B, and Pang L (2019). Sex-Related Differences in Drug-Induced QT Prolongation and Torsades de Pointes: A New Model System with Human iPSC-CMs. Toxicol. Sci 167: 360–374. [PubMed: 30247688]

Ishihara K, Sarai N, Asakura K, Noma A, and Matsuoka S (2009). Role of Mg2+ block of the inward rectifier K+ current in cardiac repolarization reserve: A quantitative simulation. J. Mol. Cell. Cardiol 47: 76–84. [PubMed: 19303883]

Jæger KH, Charwat V, Wall S, Healy KE, and Tveito A (2021). Identifying Drug Response by Combining Measurements of the Membrane Potential, the Cytosolic Calcium Concentration, and the Extracellular Potential in Microphysiological Systems. Front. Pharmacol 11: 1–16.

Johannesen L, Vicente J, Mason JW, Sanabria C, Waite-Labott K, Hong M, et al. (2014). Differentiating drug-induced multichannel block on the electrocardiogram: Randomized study of dofetilide, quinidine, ranolazine, and verapamil. Clin. Pharmacol. Ther 96: 549–558. [PubMed: 25054430]

Kernik DC, Morotti S, Wu H. Di, Garg P, Duff HJ, Kurokawa J, et al. (2019). A computational model of induced pluripotent stem-cell derived cardiomyocytes incorporating experimental variability from multiple data sources. J. Physiol 597: 4533–4564. [PubMed: 31278749]

Kernik DC, Yang PC, Kurokawa J, Wu JC, and Clancy CE (2020). A computational model of induced pluripotent stem-cell derived cardiomyocytes for high throughput risk stratification of KCNQ1 genetic variants. PLoS Comput. Biol 16: 1–28.

Keser IK (2014). Comparing two mean humidity curves using functional t-tests: Turkey case. Electron. J. Appl. Stat. Anal 7: 254–278.

Lei CL, Clerx M, Whittaker DG, Gavaghan DJ, Boer T.P. de, and Mirams GR (2020). Accounting for variability in ion current recordings using a mathematical model of artefacts in voltage-clamp experiments. Philos. Trans. A. Math. Phys. Eng. Sci 378: 20190348. [PubMed: 32448060]

Li W, Luo X, Ulbricht Y, Wagner M, Piorkowski C, El-Armouche A, et al. (2019). Establishment of an automated patch-clamp platform for electrophysiological and pharmacological evaluation of hiPSC-CMs. Stem Cell Res. 41: 101662. [PubMed: 31809994]

Lu HR, Zeng H, Kettenhofen R, Guo L, Kopljar I, Ammel K van, et al. (2019). Assessing Drug-Induced Long QT and Proarrhythmic Risk Using Human Stem-Cell-Derived Cardiomyocytes in a Ca2+ Imaging Assay: Evaluation of 28 CiPA Compounds at Three Test Sites. Toxicol. Sci 170: 345–356. [PubMed: 31020317]

Navarrete EG, Liang P, Lan F, Sanchez-Freire V, Simmons C, Gong T, et al. (2013). Screening drug-induced arrhythmia using human induced pluripotent stem cell-derived cardiomyocytes and low-impedance microelectrode arrays. Circulation 128: S3–13. [PubMed: 24030418]

Paci M, Koivumäki JT, Lu HR, Gallacher DJ, Passini E, and Rodriguez B (2021a). Comparison of the Simulated Response of Three in Silico Human Stem Cell-Derived Cardiomyocytes Models and in Vitro Data Under 15 Drug Actions. 12: 1–16.

Paci M, Koivumäki JT, Lu HR, Gallacher DJ, Passini E, and Rodriguez B (2021b). Comparison of the Simulated Response of Three in Silico Human Stem Cell-Derived Cardiomyocytes Models and in Vitro Data Under 15 Drug Actions. Front. Pharmacol 12: 1–16.

Paci M, Pölönen RP, Cori D, Penttinen K, Aalto-Setälä K, Severi S, et al. (2018). Automatic optimization of an in silico model of human iPSC derived cardiomyocytes recapitulating calcium handling abnormalities. Front. Physiol 9: 1–14. [PubMed: 29377031]

Peters CH, Liu PW, Morotti S, Gantz SC, Grandi E, Bean P, et al. (2021). Bi-directional flow of the funny current (I f) during the pacemaking cycle in murine sinoatrial node myocytes.

Pioner JM, Santini L, Palandri C, Martella D, Lupi F, Langione M, et al. (2019). Optical investigation of action potential and calcium handling maturation of hiPSC-cardiomyocytes on biomimetic substrates. Int. J. Mol. Sci 20:.

Quach B, Krogh-Madsen T, Entcheva E, and Christini DJ (2018). Light-Activated Dynamic Clamp Using iPSC-Derived Cardiomyocytes. Biophys. J 115: 2206–2217. [PubMed: 30447994]

Sager PT, Gintant G, Turner JR, Pettit S, and Stockbridge N (2014). Rechanneling the cardiac proarrhythmia safety paradigm: A meeting report from the Cardiac Safety Research Consortium. Am. Heart J 167: 292–300. [PubMed: 24576511]

Tveito A, Jæger KH, Huebsch N, Charrez B, Edwards AG, Wall S, et al. (2018). Inversion and computational maturation of drug response using human stem cell derived cardiomyocytes in microphysiological systems. Sci. Rep 8: 1–14. [PubMed: 29311619]

Woosley R, Heise C, Gallo T, Tate J, Woosley D, and KA R www.CredibleMeds.org, QTdrugs List.

Yang PC, Demarco KR, Aghasafari P, Jeng MT, Dawson JRD, Bekker S, et al. (2020). A Computational Pipeline to Predict Cardiotoxicity: From the Atom to the Rhythm. Circ. Res 947–964. [PubMed: 32091972]

Zou L, Xue Y, Jones M, Heinbockel T, Ying M, and Zhan X (2018). The Effects of Quinine on Neurophysiological Properties of Dopaminergic Neurons. Neurotox. Res 34: 62–73. [PubMed: 29285614]

Bullet point summary

What is already known

- Human induced stem cell-derived cardiomyocytes (iPSC-CMs) are used to screen for drug cardiotoxicity.
- iPSC-CMs are heterogeneous, complicating the ability to link experimental cardiotoxicity markers to drug mechanism.

What this study adds

- A model-driven, optimized, experimental protocol to detect drug cardiotoxicity markers and mechanism during iPSC-CM experiments.
- A previously unreported block of cardiac funny current by quinine.

What is the clinical significance

- A novel approach to screening for drug cardiotoxicity using human-derived cells.
- Quinine strongly blocks funny current above 3x its effective free plasma concentration.

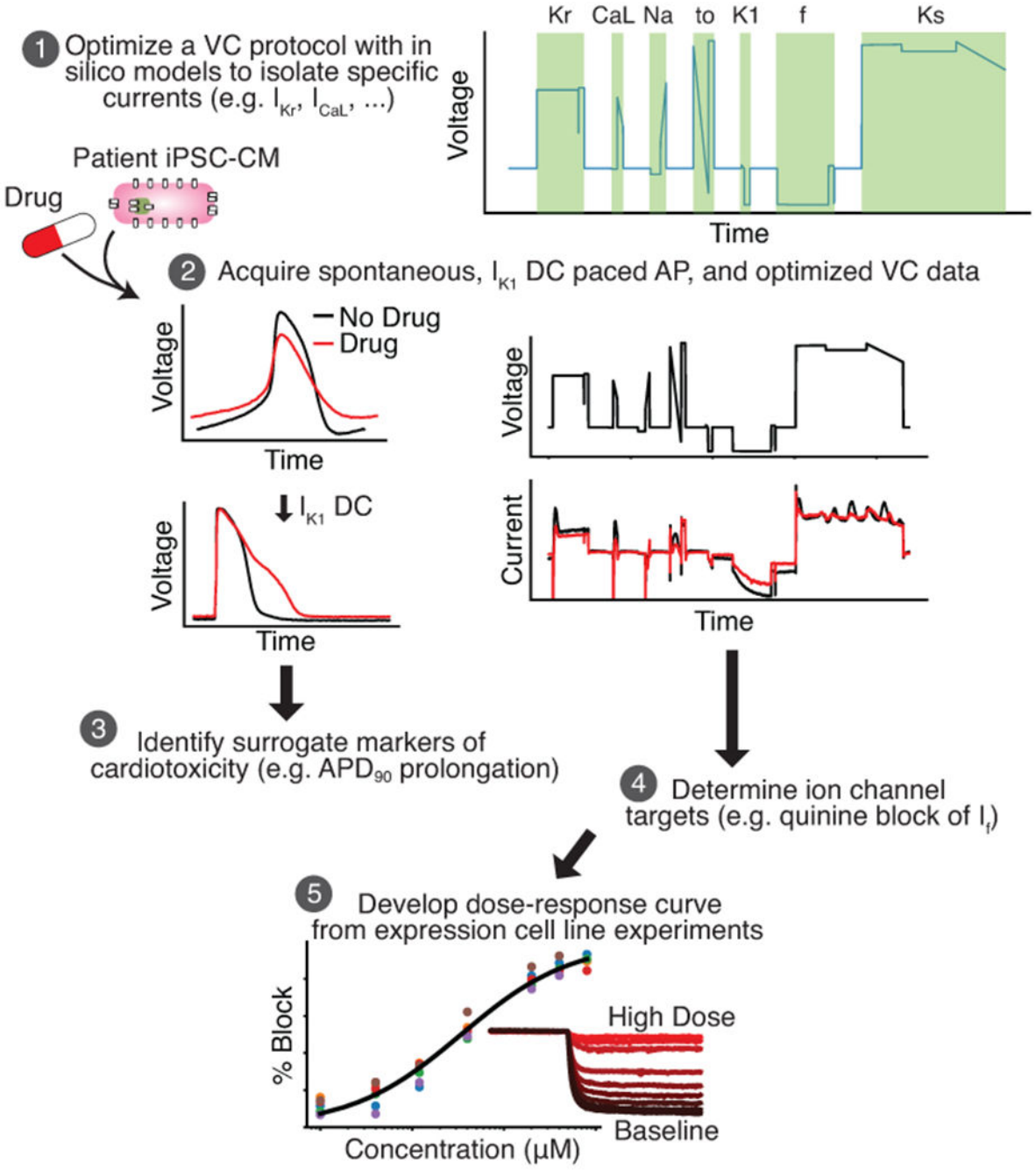

Figure 1: An *in silico-in vitro* pipeline to determine drug cardiotoxicity risk and mechanism.

Step 1, The Kernik-Clancy model with experimental artifacts is used to develop a VC protocol that is specifically designed to isolate currents. **Step 2,** Spontaneous, I_{K1} dynamic clamp and paced AP, and optimized VC data is acquired from a patient-derived iPSC-CM before and after drug application. **Step 3,** The change in I_{K1} dynamic clamp and paced AP data from pre- to post-drug application is used to identify AP prolongation, a surrogate marker of cardiotoxicity. **Step 4,** Changes in VC data is used to determine the ion channels

targeted by a drug. **Step 5,** After identifying the ion channel targeted by a drug, a dose-response curve is developed for each of these ion channels using expression line cells.

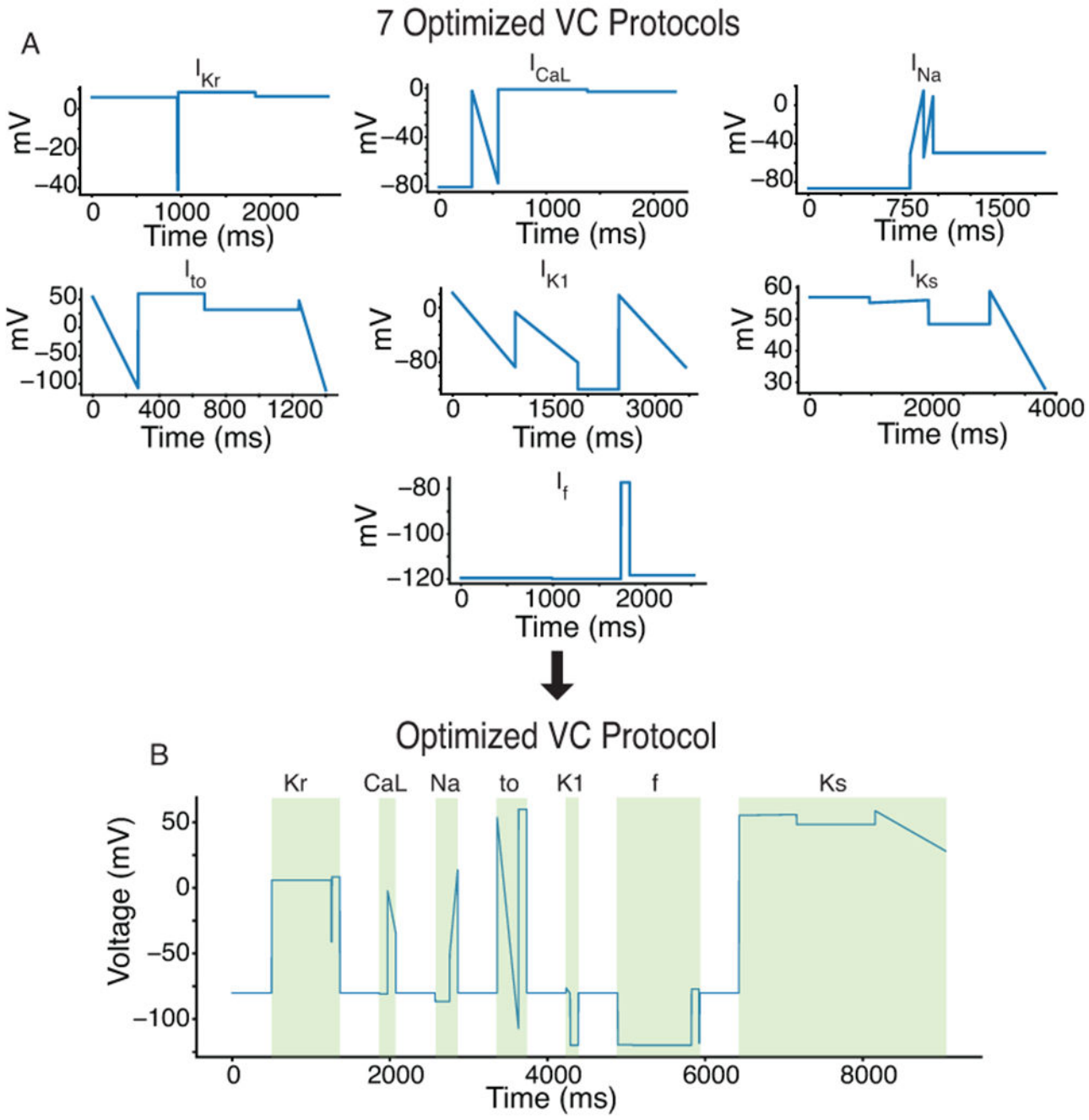

Figure 2: A GA optimized a VC protocol to isolate individual current contributions in an *in silico* iPSC-CM model.

A, The GA was used to develop individual VC protocols for seven of the most predominant ionic currents in cardiac cells. **B,** These seven protocols were systematically shortened and joined together by a −80mV holding step to produce an optimized VC protocol that isolates each of the seven currents.

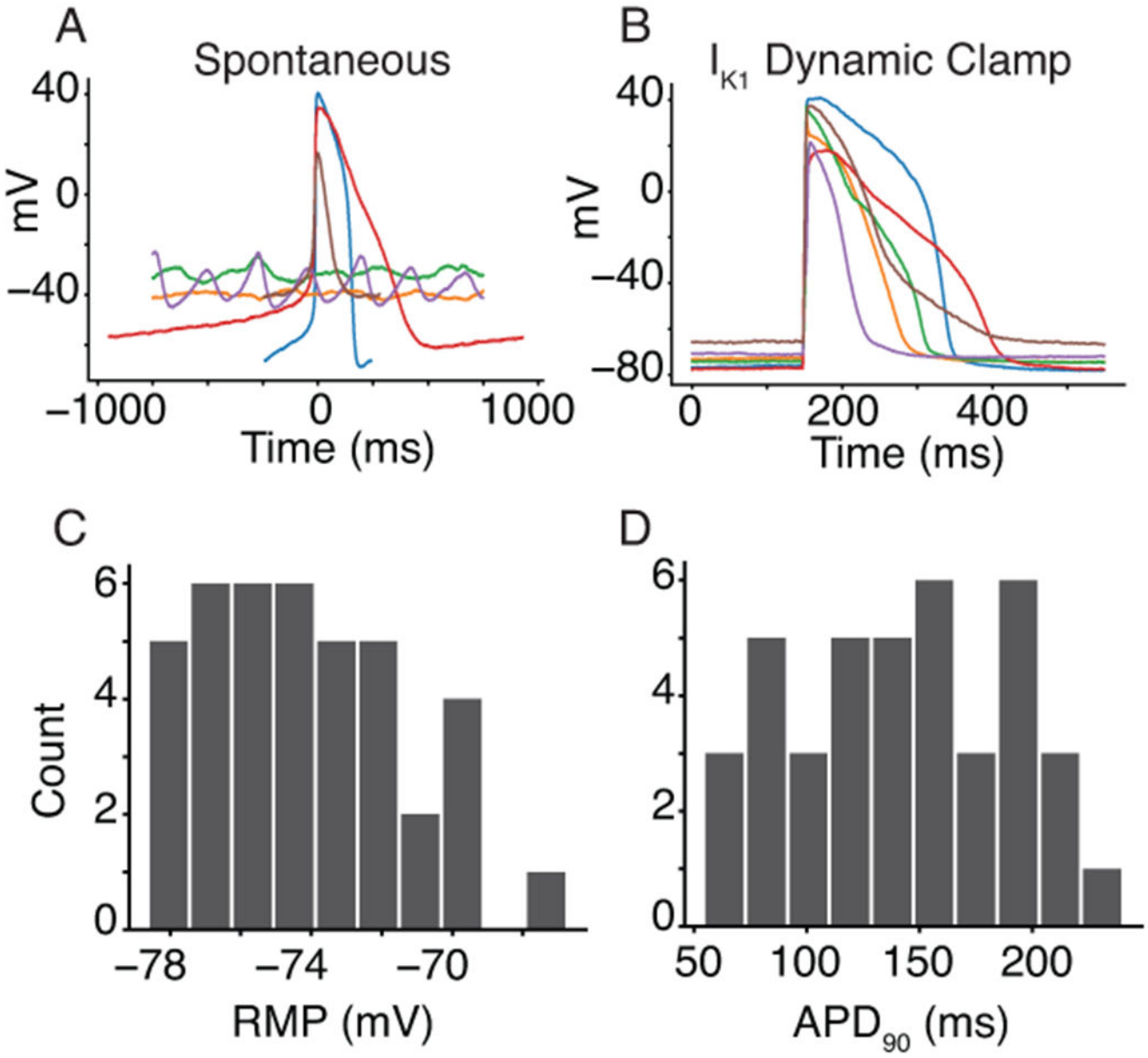

Figure 3. Synthetic maturation of iPSC-CMs with dynamically clamped I_{K1} ensures consistent APs under 1Hz pacing conditions.

A, Spontaneous behavior from a subpopulation of six cells that indicate the level of heterogeneity and inconsistent presence of APs in the cell population. **B**, I_{K1} dynamic clamp applied to the same cells makes them appear more mature when paced at 1Hz. **C and D**, Histograms for the I_{K1} dynamically clamped and paced AP resting membrane potential (−74.2 ± 2.8 mV) and action potential duration at 90% repolarization (142.0 ± 48.3 ms) for the 40 cells in this study.

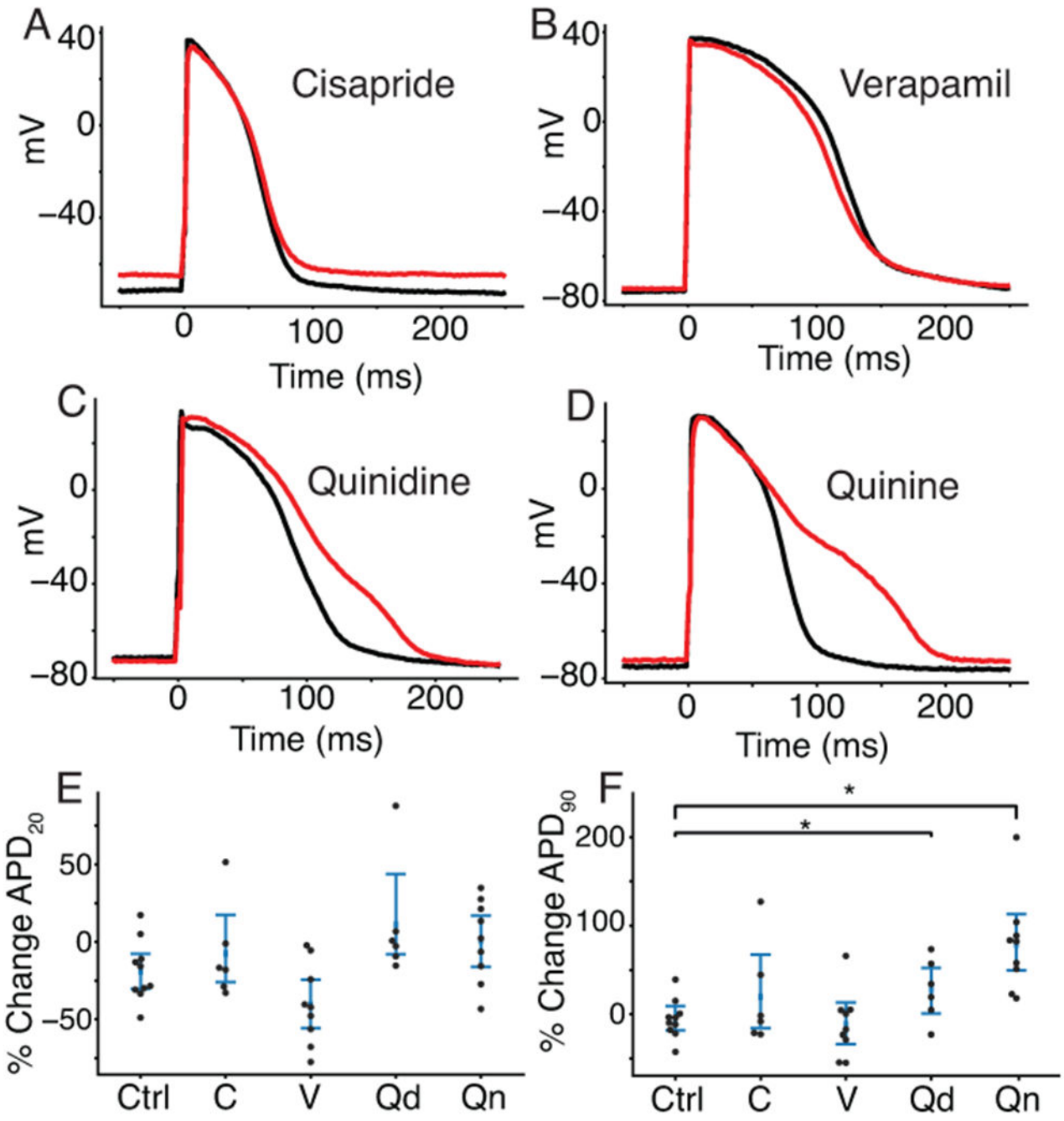

Figure 4. Drug treatment resulted in AP morphology changes consistent with the effects caused by drug block of the expected currents.

Four cells with dynamically clamped I_{K1} and paced at 1Hz before (black) and after (red) treatment with cisapride (**A**), verapamil (**B**), quinidine (**C**), and quinine (**D**). **E**, Percent change in APD_{20} and (**F**) APD_{90} for drugs treated with cisapride (labeled C), verapamil (V), quinidine (Qd), quinine (Qn) or a DMSO control solution (Ctrl). No drugs caused a significant change in APD_{20} compared to control cells. Quinidine (p=.034) and quinine (Qn, p=.0003) showed significant prolongation when compared to control cells.

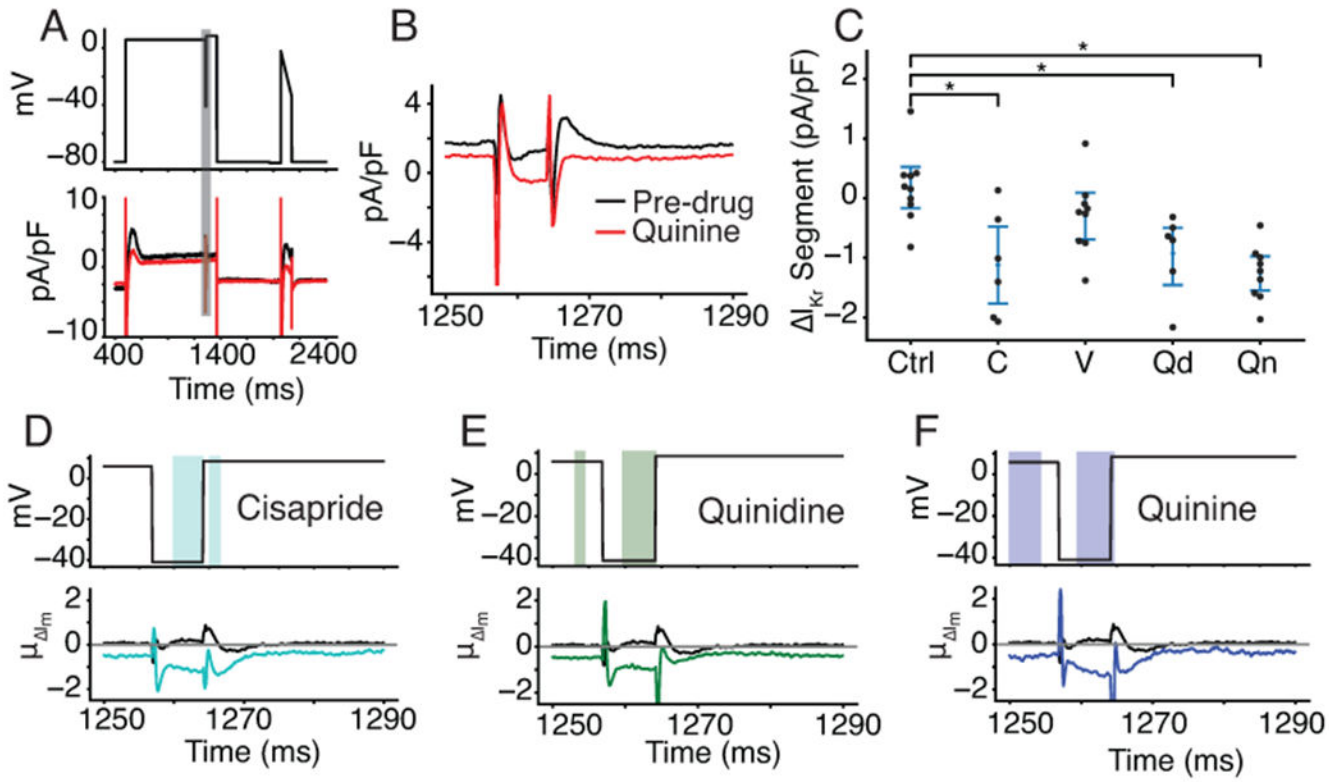

Figure 5. Optimized VC protocol correctly identifies I_{Kr} as a target of cisapride, quinidine, and quinine.

A, Representative cell shows the effect of quinine on the current response during the segment of the VC protocol designed to isolate I_{Kr}. The black trace is pre-drug and the red trace is post-drug. **B**, the current trace during the segment meant to isolate I_{Kr} (shaded grey in panel A). **C**, Cells treated with cisapride (labeled C, p=.0032), quinidine (labeled Qd, p=.0041), and quinine (labeled Qn, p=.00002) show a decrease in total current during the VC segment designed to isolate I_{Kr}. At the concentrations used in this experiment, cisapride, quinidine, and quinine should block 95%, 89%, and 72% of I_{Kr}, respectively. **D**, **E**, and **F**, Functional t-tests show a significant difference in the average change in current during the I_{Kr}-isolating segment when comparing cells treated with DMSO to cells treated with cisapride (**D**), quinidine (**E**), and quinine (**F**). Verapamil was excluded because there was no significant difference during this segment of the protocol.

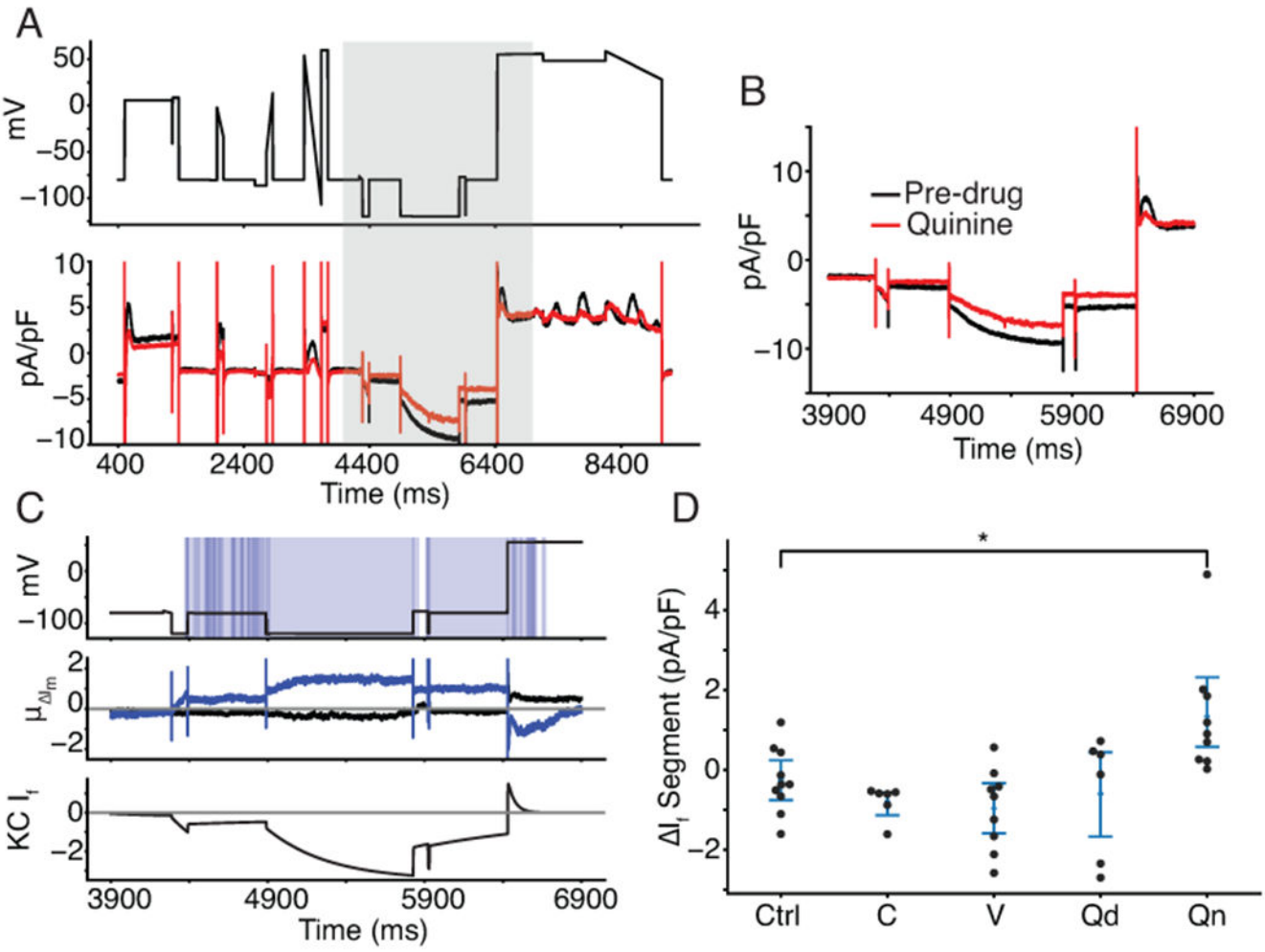

Figure 6: VC protocol identifies funny current as a target of quinine.

A, Representative cell treated with quinine shows a reduction in inward current when the cell is clamped to a hyperpolarized potential of −120 mV, before 6000 ms. After 6000 ms, outward current is reduced as I_f reverses in direction before inactivating. **B**, the current trace during and around the segment meant to isolate I_f (shaded grey in panel A). **C**, Functional t-test shows a significant difference between quinine-treated cells and control cells throughout the period of the protocol when funny current would be active (**C**, **top**). The average difference between quinine-treated and control cells is between 0.8 and 1.2 pA/pF throughout this period (**C**, **middle**). The Kernik-Clancy iPSC-CM model funny current becomes active during the period when quinine-treated cells show a significant change in current and turns off just before the p value increases above .05 (**C, bottom**). **D**, Cells treated with quinine (labeled Qn, p=.0097) show a decrease in total current during the VC segment designed to isolate I_f.

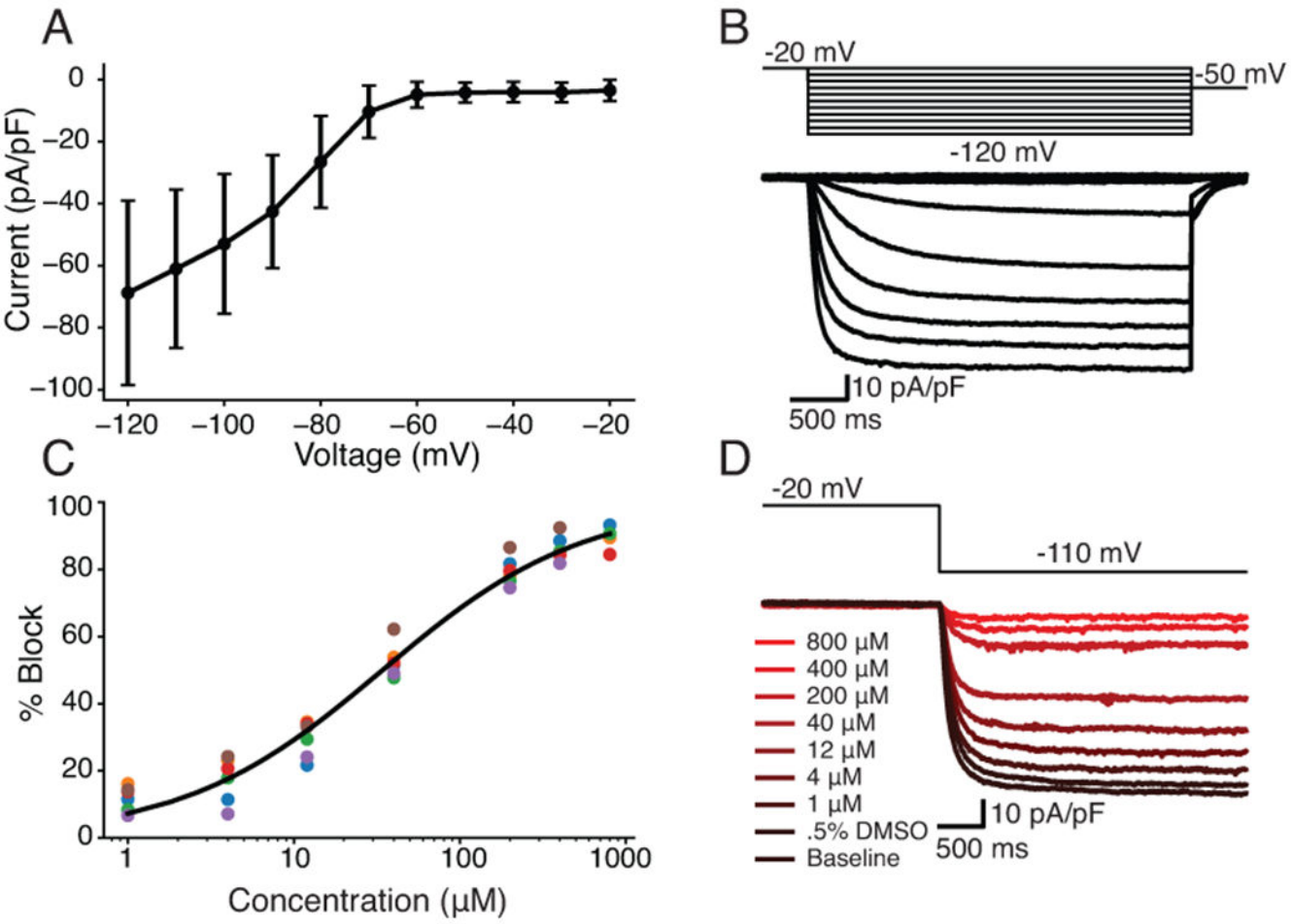

Figure 7: Dose-response curve shows quinine block of funny current in HEK-293 cells stably expressing HCN1.

A, IV curve with averages and errors calculated from six HEK-HCN1 cells. **B**, Representative HEK-HCN1 current-voltage traces. **C**, Dose-response curve fit to pharmacology data from six HEK-HCN1 cells. **D**, Traces generated from a representative cell by clamping at −20mV for 3000ms, and then stepping to −110mV for 3500ms at all tested concentrations.

Table 1:

The optimized VC protocol correctly identifies strong drug blocks

Drug	I_{Kr}	I_{CaL}	I_{Na}	I_{to}	I_{K1}	I_f	I_{Ks}
Cisapride (125 nM)	95%*	1%	2%	13%	5%	??	2%
Verapamil (150 nM)	21%	39% *	<1%	1%	3%	??	3%
Quinidine (2,529 nM)	89%*	16%	10%	43%*	1%	??	27%
Quinine (12,000 nM)	72%*	29%	28%	15%	<1%	32%*†	20%

All percent block data, except quinine block of I_f, is taken from Crumb et al. (2016). The quinine block of I_f is from the HEK-HCN1 experiments in this study. The optimized VC protocol qualitatively identifies drug blocks that Crumb et al. showed were greater than 30%

(* indicates $p<0.05$) and identifies funny current as a target of quinine (†).